A modulated gradient model for scalar transport in large-eddy simulation of the atmospheric boundary layer

Hao Lu,[1, 2, *] Fernando Porté-Agel[1, 2, †]

[1]Wind Engineering and Renewable Energy Laboratory (WIRE),

École Polytechnique Fédérale de Lausanne (EPFL), CH-1015 Lausanne, Switzerland

[2]Saint Anthony Falls Laboratory, University of Minnesota - Twin Cities,

2 Third Ave SE, Minneapolis, MN 55414, USA

Abstract

As a simple alternative to the standard eddy-diffusivity closure, a nonlinear subgrid-scale (SGS) flux model is introduced and implemented in simulations of a neutral atmospheric boundary layer and a stable atmospheric boundary layer. The new model computes the structure of the SGS flux (relative magnitude of the vector components) based on the normalized gradient vector, which is derived from the Taylor expansion of the exact SGS flux. The SGS magnitude is computed as the product of a SGS velocity scale and a SGS scalar concentration scale, which are estimated based on the local-equilibrium hypothesis. To resolve the instability issue of the original gradient model and ensure numerical stability, we adopt a clipping procedure to avoid local negative SGS dissipation rate of the scalar variance. The model formulation using constant coefficients is assessed through a systematic comparison with well-established theoretical predictions and reference results of various flow statistics. Simulation results obtained with the use of this new model show good agreement with the reference results and an evident improvement over results obtained using traditional eddy-diffusivity models. For instance, the new model can deliver the expected surface-layer similarity scalar profile and power-law scaling of the power spectrum of scalar fluctuation.

*E-mail: hao.lu@live.com

†E-mail: fernando.porte-agel@epfl.ch

1 Introduction

Large-eddy simulation (LES) is a useful tool for the study of high-Reynolds-number turbulent flows. The physical basis for LES is the separation of the flow into resolved and subgrid-scale (SGS) motions. This is achieved through the use of a three-dimensional spatial filtering operation, denoted here as a tilde ($\widetilde{\ }$). The resolved (filtered) motions contain most of the energy, and one can compute them numerically by solving the filtered governing equations, while the effects of the less energetic SGS motions are parameterized. This study is devoted to the extension of a recently introduced SGS stress model (Lu and Porté-Agel, 2010) dealing with the LES of turbulent atmospheric boundary layer (ABL) flows to the case where a scalar is introduced into the flow. The closure problem is restricted to the spatially filtered scalar transport equation, and effects of the SGS motions are represented by the divergence of the SGS flux vector. The SGS flux vector is defined as

$$q_i = \widetilde{u_i\theta} - \widetilde{u}_i\widetilde{\theta} \ , \tag{1}$$

and it must be closed in terms of the resolved velocity field $\widetilde{u}_i$ and the resolved scalar field $\widetilde{\theta}$.

Numerous SGS models have been proposed since the introduction of the first SGS stress model by Smagorinsky (1963). The Smagorinsky model belongs to the family of eddy-viscosity and eddy-diffusivity models. They all rest on two important assumptions: (i) the effects of the SGS motions on the resolved motions are essentially energetic actions, so that the modeling focuses primarily on the balance of the energy transfers between the two scale ranges, and (ii) the energy-transfer mechanism is analogous to the molecular mechanism represented by diffusion. The local-equilibrium hypothesis is often adopted to determine the model coefficients. In the context of ABL flows, the early eddy-viscosity/diffusivity models have revealed that the mean wind and temperature profiles in the surface layer differ from the Monin-Obukhov similarity forms (e.g., Businger et al., 1971; Stull, 1988). Specifically, the nondimensional vertical gradients of velocity and temperature could be overestimated by more than 20% in the surface layer. To try and resolve this issue, researchers have introduced quite a few modifications for different aspects of ABL flows. For instance, Mason (1989) and Mason and Thomson (1992) used an *ad-hoc* expression to provide proper SGS mixing lengths; Sullivan et al. (1994) proposed a two-part eddy-viscosity/diffusivity model that includes contributions from the mean flow; Kosović (1997) proposed a nonlinear modification that allows backward energy cascade; and Porté-Agel et al. (2000) and Porté-Agel (2004) used a scale-dependent dynamic approach to compute the model coefficients dynamically, while allowing for scale-dependence of the coefficients.

The variety of SGS models for simulating ABL flows arises not only because the theoretical justifications are arguable but also because LES solutions are sensitive to the given type of SGS models, especially in the surface layer. In contrast to eddy-viscosity/diffusivity models,

gradient models are derived from the Taylor series expansions of the SGS terms that appear in the filtered conservation equations (Clark et al., 1979), do not locally assume the same eddy viscosity/diffusivity for all directions, and make no use of prior knowledge of the interactions between resolved motions and SGS motions. At *a-priori* level, gradient models generally predict the structure of the exact SGS terms much more accurately than eddy-viscosity/diffusivity models (and therefore are better able to capture anisotropic effects and disequilibrium, e.g., Liu et al., 1994; Higgins et al., 2003; Porté-Agel et al., 2001; Lu et al., 2007). These features make gradient models attractive. However, when implemented in LESs, they are not able to yield the correct levels of the SGS kinetic energy production (energy transfer between resolved and SGS scales), and as a result, simulations often become numerically unstable as reported in a variety of contexts (e.g., Sagaut, 2006).

Different schemes have been introduced for resolving this insufficient-dissipation issue. Bardina et al. (1980) proposed a mixed procedure; and later on, Chow et al. (2005) showed that this procedure delivers good agreement with similarity theory in LES of neutral ABL flows. Vreman et al. (1996, 1997) and Lu et al. (2008) mixed gradient terms with $O(\widetilde{\Delta}^2)$ and $O(\widetilde{\Delta}^4)$ eddy-viscosities to simulate different types of turbulent flows, and showed that mixed gradient models are capable of capturing disequilibrium and anisotropy effects. Liu et al. (1994) revisited this energy cascade issue and recommended another meaningful choice, a clipping procedure, to control the amplitude of backward cascade induced by the model. Inconveniently, Vreman et al. (1997) have reported that their coupling of the gradient model with the clipping procedure still does not provide sufficient SGS dissipation in simulations of mixing layer flows.

A recent effort (Lu and Porté-Agel, 2010) adopted a new SGS model formulation for the LES of ABL flows that builds on the work of Pomraning and Rutland (2002) and Lu et al. (2007, 2008). This model for the SGS stress tensor, $\tau_{ij} = \widetilde{u_i u_j} - \widetilde{u}_i \widetilde{u}_j$, can be written as

$$\tau_{ij} = 2k_{sgs} \left(\frac{\widetilde{G}_{ij}}{\widetilde{G}_{kk}} \right) \ , \tag{2}$$

where $k_{sgs} = \frac{1}{2}\tau_{ii}$ is the SGS kinetic energy, and $\widetilde{G}_{ij}$ is the gradient tensor, which is defined as $\widetilde{G}_{ij} = \frac{\widetilde{\Delta}^2}{12}\left(\frac{\partial \widetilde{u}_i}{\partial x_k}\frac{\partial \widetilde{u}_j}{\partial x_k}\right)$ for a three-dimensional isotropic filter of size $\widetilde{\Delta}$ (e.g., Sagaut, 2006), and $\widetilde{G}_{ij} = \frac{\widetilde{\Delta}_x^2}{12}\frac{\partial \widetilde{u}_i}{\partial x}\frac{\partial \widetilde{u}_j}{\partial x} + \frac{\widetilde{\Delta}_y^2}{12}\frac{\partial \widetilde{u}_i}{\partial y}\frac{\partial \widetilde{u}_j}{\partial y} + \frac{\widetilde{\Delta}_z^2}{12}\frac{\partial \widetilde{u}_i}{\partial z}\frac{\partial \widetilde{u}_j}{\partial z}$ for anisotropic filters/grids (for which $\widetilde{\Delta}_x$, $\widetilde{\Delta}_y$ and $\widetilde{\Delta}_z$ are not equal) such as the ones considered in this study. Through the formulation, the structure (the relative magnitude of the different components) of the SGS stress tensor is modeled by the normalized gradient tensor, and the magnitude of the SGS stress tensor is modeled by an estimation of k_{sgs}. The nonlinear model formulation has been shown to improve the modeling of energy transfers at intermediate scales and deliver better flow statistics, such as energy decay rate and flow structure (Lu et al., 2007, 2008; Rutland, 2011). Lu and Porté-Agel (2010)

adopted the local-equilibrium hypothesis, which assumes a balance between the SGS kinetic energy production P ($P = -\tau_{ij}\widetilde{S}_{ij}$, where $\widetilde{S}_{ij} = \frac{1}{2}\left(\frac{\partial \widetilde{u}_i}{\partial x_j} + \frac{\partial \widetilde{u}_j}{\partial x_i}\right)$ is the resolved strain rate tensor) and dissipation rate (classically modeled as $\varepsilon = C_\varepsilon \frac{k_{sgs}^{3/2}}{\widetilde{\Delta}}$). A clipping procedure is used to assure that the SGS dissipation rate is non-negative, and thus

$$k_{sgs} = H\left(P\right) \frac{4\widetilde{\Delta}^2}{C_\varepsilon^2} \left(-\frac{\widetilde{G}_{ij}}{\widetilde{G}_{kk}} \widetilde{S}_{ij} \right)^2 , \tag{3}$$

where $H(x)$ is the Heaviside step function defined as $H(x) = 0$ if $x < 0$ and $H(x) = 1$ if $x \geq 0$. The model has been assessed through a systematic comparison with well-established empirical formulations and theoretical predictions of a variety of flow statistics in a neutral ABL. It is capable of reproducing the expected log-law mean velocity profile and power-law energy spectra, and simulations yield streaky structures and near-Gaussian probability density functions of velocity in the surface layer. A further assessment study showed that, in decaying isotropic turbulences, the clipping is applied less than 30% of time and produces no strong energy jumps; also the model is capable of achieving reasonable spectra, as well as other key statistical characteristics (Lu, 2011). After the encouraging performance of this simple SGS stress model, an extension of this approach to modeling the SGS scalar flux appears interesting.

The scalar problem is a key component of many turbulent flows, and of ABL flows in particular. However, the extension of SGS stress models to scalar flux is not obvious. In this paper, we focus on the development of a simple alternative to the standard eddy-diffusivity closure, and propose (in section 2) a computationally inexpensive modulated gradient model that uses the local-equilibrium hypothesis to estimate the SGS velocity scale and the SGS scalar concentration scale. The model features a clipping procedure for avoidance of negative dissipation. We test the performance of the modulated gradient model in high-Reynolds-number simulations of a neutrally stratified ABL case and a stably stratified ABL case. Section 3 describes the governing equations and common numerical setup. Section 4 and section 5 present the LES results. Section 6 summarizes the findings.

2 The modulated gradient model

Our proposed SGS flux vector model is written as

$$q_i = |\mathbf{q}| \left(\frac{\widetilde{G}_{\theta,i}}{|\widetilde{\mathbf{G}}_\theta|} \right) . \tag{4}$$

This formulation separates the modeling into two elements: the normalized gradient vector serves to model the structure (relative magnitude in each direction) of the SGS flux vector;

and a separate model is needed for the magnitude of the SGS flux. To account for the grid anisotropy, the gradient vector is computed as $\widetilde{G}_{\theta,i} = \frac{\widetilde{\Delta}_x^2}{12}\frac{\partial \widetilde{u}_i}{\partial x}\frac{\partial \widetilde{\theta}}{\partial x} + \frac{\widetilde{\Delta}_y^2}{12}\frac{\partial \widetilde{u}_i}{\partial y}\frac{\partial \widetilde{\theta}}{\partial y} + \frac{\widetilde{\Delta}_z^2}{12}\frac{\partial \widetilde{u}_i}{\partial z}\frac{\partial \widetilde{\theta}}{\partial z}$, and we compute its magnitude with the Euclidean norm $|\widetilde{\mathbf{G}}_\theta| = \sqrt{\widetilde{G}_{\theta,1}^2 + \widetilde{G}_{\theta,2}^2 + \widetilde{G}_{\theta,3}^2}$. To close this model, we need to evaluate the magnitude of the SGS flux vector, $|\mathbf{q}|$.

Even though a previous approach (Chumakov and Rutland, 2005) places much emphasis on the scalar field, it is desirable, owing to the definition of the SGS flux vector as shown in equation (1), that the SGS flux magnitude encompasses both the velocity and the scalar fields. Therefore here we propose to model the flux magnitude as the multiplication of an SGS velocity scale and an SGS scalar concentration scale

$$|\mathbf{q}| = u_{sgs}\theta_{sgs} \ . \tag{5}$$

It is straightforward to assume that the SGS velocity scale is proportional to the square root of the SGS kinetic energy, $u_{sgs} = C\sqrt{k_{sgs}}$. Further, we adopt the local-equilibrium hypothesis to estimate the SGS scalar concentration scale. This hypothesis constitutes the basic assumption of many SGS approaches, such as the Smagorinsky model (Smagorinsky, 1963) and many other models (e.g., Germano et al., 1991; Moin et al., 1991; Pierce and Moin, 1998; Knaepen et al., 2002; Lu and Porté-Agel, 2010). Especially, as the most commonly used method in engineering and other fields, dynamic Smagorinsky-type models (e.g., Germano et al., 1991; Moin et al., 1991) adopt this hypothesis as well as the scale-invariance assumption to determine model coefficients as functions of space and time. Although several studies (e.g., Borue and Orszag, 1998; da Silva and Métais, 2002; Park et al., 2006; You and Moin, 2007) pointed that this hypothesis does not hold very well locally, it does work better for the scalar than for the velocity field (e.g., da Silva and Pereira, 2005). The hypothesis assumes a balance between the SGS scalar variance production, $P_\theta = -q_i\frac{\partial \widetilde{\theta}}{\partial x_i}$, and the SGS scalar variance dissipation rate ε_θ, which is evaluated by a classical method, $\varepsilon_\theta = C_{\varepsilon\theta}\frac{\theta_{sgs}^2 u_{sgs}}{\widetilde{\Delta}}$. Note that various models for the SGS scalar variance dissipation rate exist (e.g., Girimaji and Zhou, 1996; Sanders and Gökalp, 1998; Chumakov and Rutland, 2005; Balarac et al., 2008a), but a recent study (da Silva et al., 2008) has shown that the classical models (i.e., $\varepsilon = C_\varepsilon\frac{k_{sgs}^{3/2}}{\widetilde{\Delta}}$ and $\varepsilon_\theta = C_{\varepsilon\theta}\frac{\theta_{sgs}^2 u_{sgs}}{\widetilde{\Delta}}$) give good results in terms of topology, spatial localization, statistical behavior and spectral characteristics. A clipping procedure ensures the dissipation rate is non-negative, thus

$$\theta_{sgs} = H\left(P_\theta\right)\frac{\widetilde{\Delta}}{C_{\varepsilon\theta}}\left(-\frac{\widetilde{G}_{\theta,i}}{|\widetilde{\mathbf{G}}_\theta|}\frac{\partial \widetilde{\theta}}{\partial x_i}\right) \ . \tag{6}$$

An alternative method to evaluate the SGS scalar concentration scale could be the square root of the SGS scalar variance. We have tested several combinations of models of the SGS kinetic energy (Knaepen et al., 2002; Yoshizawa and Horiuti, 1985; Yoshizawa, 1986; You and Moin,

2007) and the SGS scalar variance (Pierce and Moin, 1998; Chumakov and Rutland, 2005; Balarac et al., 2008b), and found many of them do not provide sufficient dissipation. It should also be mentioned that these combinations are much more sophisticated and computationally expensive than the proposed formulation. In this study, we focus on the development of a simple alternative to the standard eddy-diffusivity closure, and thus propose a computationally inexpensive modulated gradient model that uses the local-equilibrium hypothesis to estimate the SGS scales.

A dynamic procedure (Germano et al., 1991; Lilly, 1992) might serve to determine the model coefficient $C_{\varepsilon\theta}$; but, for simplicity, here we adopt assumptions to justify a simple method for determining a constant value. It has been assumed by Jiménez et al. (2001), in a study of the SGS scalar variance dissipation, that the SGS scalar mixing time is proportional to the SGS turbulent characteristic time. Tests have shown that a satisfactory ratio is the Schmidt number (or the Prandtl number depending on the physical significance of the scalar field), in terms of, $\frac{\theta_{sgs}^2}{\varepsilon_\theta} : \frac{k_{sgs}}{\varepsilon} = Sc$. Then, the coefficient can be derived as $C_{\varepsilon\theta} = \frac{1}{Sc}\frac{C_\varepsilon}{C}$, and the magnitude of the SGS flux can be expressed as

$$|\mathbf{q}| = H\left(P_\theta\right) H\left(P\right) \frac{1}{Sc} \frac{2\widetilde{\Delta}^2}{C_{\varepsilon\theta}^2} \left(-\frac{\widetilde{G}_{\theta,i}}{|\widetilde{\mathbf{G}}_\theta|} \frac{\partial \widetilde{\theta}}{\partial x_i} \right) \left(-\frac{\widetilde{G}_{ij}}{\widetilde{G}_{kk}} \widetilde{S}_{ij} \right) \ . \tag{7}$$

When adopting (as this study has done) $Sc = 0.71$ (the Prandtl number of air near 20°C), $C_\varepsilon = 1$ (e.g., Yoshizawa and Horiuti, 1985; Kim and Menon, 1995), and $C = \sqrt{2}$ (with $u_{sgs} = \sqrt{\widetilde{u_i u_i} - \widetilde{u}_i \widetilde{u}_i} = \sqrt{2\, k_{sgs}}$), one obtains $C_{\varepsilon\theta} = 1.0$. In this paper, the combination of the SGS stress model described in equations (2) and (3) and this SGS flux vector model is abbreviated as "MGM."

3 Numerical simulations

Previous studies (e.g., Andren et al., 1994; Sullivan et al., 1994) have stated that the discrepancy between simulation results and surface-layer similarity theory becomes more evident as surface buoyancy forcing decreases. In this regard, one should expect a larger impact of the SGS formulation in neutral and stable cases than in convective (unstable) cases. The current paper focuses on two cases: one involves neutral stability conditions, and another involves stably stratified conditions. Also, because the simulated flows bear high Reynolds numbers (commonly $O(10^8)$ or larger), no near-wall viscous processes are resolved, and the viscous terms ($\sim 1/10^{10}$ of the SGS terms at the resolution of 128^3) are neglected in the governing equations.

We use a modified LES code that has been used for previous studies (e.g., Albertson and Parlange, 1999; Porté-Agel et al., 2000; Porté-Agel, 2004; Stoll and Porté-Agel, 2006a,b, 2008;

Lu and Porté-Agel, 2010). The code solves the filtered equations of continuity, conservation of momentum and scalar transport

$$\frac{\partial \widetilde{u}_i}{\partial x_i} = 0 \,, \tag{8}$$

$$\frac{\partial \widetilde{u}_i}{\partial t} + \frac{\partial \widetilde{u}_i \widetilde{u}_j}{\partial x_j} = -\frac{\partial \widetilde{p}}{\partial x_i} - \frac{\partial \tau_{ij}}{\partial x_j} + \widetilde{f}_i \,, \tag{9}$$

$$\frac{\partial \widetilde{\theta}}{\partial t} + \widetilde{u}_i \frac{\partial \widetilde{\theta}}{\partial x_i} = -\frac{\partial q_i}{\partial x_i} \,, \tag{10}$$

where $(\widetilde{u}_1, \widetilde{u}_2, \widetilde{u}_3) = (\widetilde{u}, \widetilde{v}, \widetilde{w})$ are the components of the resolved velocity field, $\widetilde{\theta}$ is the resolved scalar, $\widetilde{p}$ is the effective pressure, and $\widetilde{f}_i$ is a forcing term. In the stable case, the buoyancy force and the Coriolis force would be included as $\widetilde{f}_i = \delta_{i3} g \frac{\widetilde{\theta} - \langle \widetilde{\theta} \rangle_H}{\theta_0} + f_c \varepsilon_{ij3} \widetilde{u}_j$, where $\widetilde{\theta}$ represents the resolved potential temperature, θ_0 is the reference temperature, $\langle \cdot \rangle_H$ denotes a horizontal average, g is the gravitational acceleration, f_c is the Coriolis parameter, δ_{ij} is the Kronecker delta, and ε_{ijk} is the alternating unit tensor.

The simulated ABLs are horizontally homogeneous. The horizontal directions are discretized pseudo-spectrally, and vertical derivatives are approximated with second-order central differences. The height of the computational domain is H, and the horizontal dimensions are L_x and L_y. The domain is divided into N_x, N_y, and N_z uniformly spaced grid points. The grid planes are staggered in the vertical direction with the first vertical velocity plane at a distance $\Delta z = \frac{H}{N_z - 1}$ from the surface, and the first horizontal velocity plane $\frac{\Delta z}{2}$ from the surface. At the bottom, the instantaneous wall stresses are computed through the application of the Monin-Obukhov similarity theory (e.g., Porté-Agel et al., 2000; Porté-Agel, 2004): $\tau_{i3}|_w = -u_*^2 \frac{\widetilde{u}_i}{U(z)} = -\left(\frac{U(z)\,\kappa}{\ln(z/z_0) - \Psi_M} \right)^2 \frac{\widetilde{u}_i}{U(z)}$, where κ is the von Kármán constant, u_* is the friction velocity, z_0 is the roughness length, Ψ_M is the stability correction for momentum, and $U(z)$ is the plane averaged resolved horizontal velocity. We compute the filter size using a common formulation $\widetilde{\Delta} = \sqrt[3]{\Delta x\, \Delta y\, \Delta z}$, where $\Delta x = \frac{L_x}{N_x}$ and $\Delta y = \frac{L_y}{N_y}$. The corresponding aliasing errors are corrected in the nonlinear terms according to the 3/2 rule (e.g., Canuto et al., 1988). The time advancement is carried out using a second-order-accurate Adams-Bashforth scheme (e.g., Canuto et al., 1988).

4 Neutral atmospheric boundary layer

The numerical setup is classical and has been used for previous model assessment studies (e.g., Porté-Agel et al., 2000; Porté-Agel, 2004; Lu and Porté-Agel, 2010). The height of the computational domain is $H = 1000\,[\mathrm{m}]$, and the horizontal dimensions of the simulated volume are $L_x = L_y = 2\pi H$. We carried out simulations with resolutions of $N_x \times N_y \times N_z = 32 \times 32 \times 32$,

$48 \times 48 \times 48$, $64 \times 64 \times 64$, $96 \times 96 \times 96$, and $128 \times 128 \times 128$. The simulated flow is driven by a constant pressure gradient $-u_*^2/H$ in the x-direction. We take the setup of $u_* = 0.45\,[\mathrm{m/s}]$ and $z_0 = 0.1\,[\mathrm{m}]$, which is similar to the setup in some previous studies (e.g., Andren et al., 1994; Porté-Agel et al., 2000; Lu and Porté-Agel, 2010). The upper boundary conditions are $\partial\widetilde{u}/\partial z = 0$, $\partial\widetilde{v}/\partial z = 0$, $\widetilde{w} = 0$ and $\partial\widetilde{\theta}/\partial z = 0$. At the bottom, the neutral stability results in $\Psi_M = 0$. A passive scalar field, similar to the one simulated in previous studies (e.g., Andren et al., 1994; Kong et al., 2000; Porté-Agel, 2004), is introduced into the simulations by imposing a constant downward surface flux $q_3|_w = -u_*\theta_*$, and we employ $\theta_* = 0.9\,[\mathrm{K}]$.

Considering that the main novelty of the proposed model comes from the fact that it does not use the eddy-viscosity/diffusivity approach, for comparison, here we also present results obtained using an eddy-viscosity/diffusivity approach of similar level of complexity (zero-equation, non-dynamic) and computational cost. The eddy-viscosity/diffusivity approach in LES consists of computing the SGS stress' deviatoric part and the SGS flux as: $\tau_{ij} - \frac{1}{3}\delta_{ij}\tau_{kk} = -2\nu_t\widetilde{S}_{ij}$, and $q_i = -\frac{\nu_t}{Sc_{sgs}}\frac{\partial\widetilde{\theta}}{\partial x_i}$, where ν_t is the SGS eddy viscosity and Sc_{sgs} is the SGS Schmidt number. Smagorinsky (1963) proposed the first SGS eddy-viscosity model; in particular, the eddy viscosity is given by $\nu_t = \left(C_s\widetilde{\Delta}\right)^2|\widetilde{S}|$, where $|\widetilde{S}| = \sqrt{2\widetilde{S}_{ij}\widetilde{S}_{ij}}$ is the strain rate and C_s is the Smagorinsky coefficient. In isotropic turbulence, if a cut-off filter is used in the inertial subrange and the filter scale $\widetilde{\Delta}$ is equal to the grid size, then $C_s \approx 0.17$ and $Sc_{sgs} \approx 0.5$ (Lilly, 1967; Antonopoulos-Domis, 1981). However, flow anisotropy, particularly the presence of a strong mean shear near the surface in high-Reynolds-number ABLs, makes the optimum values of those coefficients depart from their isotropic counterparts (e.g., Porté-Agel et al., 2001; Kleissl et al., 2003; Bou-Zeid et al., 2008). A common practice is to specify the coefficients in an *ad-hoc* fashion. The *ad-hoc* damping function proposed by Mason and Thomson (1992) can be rewritten (Porté-Agel et al., 2000) as: $C_s = \left(C_0^{-n} + \left(\kappa\left(\frac{z}{\widetilde{\Delta}} + \frac{z_0}{\widetilde{\Delta}}\right)\right)^{-n}\right)^{-1/n}$, where n is an adjustable parameter, and studies (e.g., Mason and Thomson, 1992; Andren et al., 1994; Porté-Agel et al., 2000) have reported that this formulation with values of C_0 ranging from 0.1 to 0.3, and $n = 1$, 2, or 3 can deliver a more realistic logarithmic velocity profile in the surface layer than does the standard Smagorinsky model using a constant coefficient. Studies (e.g., Mason, 1989; Mason and Thomson, 1992; Andren et al., 1994) have found the range of Sc_{sgs} is from 0.33 to 0.7. In line with the study by Porté-Agel et al. (2000), we adopt the damping coefficients for the model with $C_0 = 0.17$ and $n = 1$ (this modified Smagorinsky model is abbreviated as "MSM"), and adopt the two constant values of $Sc_{sgs} = 0.7$ (Mason and Thomson, 1992; Andren et al., 1994), and $Sc_{sgs} = 0.5$ (Mason, 1989).

We have collected mean and turbulent statistics after achieving statistically steady states. In the presentation, we denote the horizontal and time average as $< \cdot >$, and the fluctuation of an arbitrary resolved variable $\widetilde{f}$ as $\widetilde{f}' = \widetilde{f} - < \widetilde{f} >$; and on certain occasions, we take the

simulations of 64^3-node and 128^3-node as base cases to present results.

4.1 First-order measurements

A long-standing problem in the LES of ABL flows is that the mean wind and temperature profiles differ from the similarity forms in the surface layer. In this subsection, we compare our numerical results with the predictions from similarity theory to gain a better understanding of the performance of the new model.

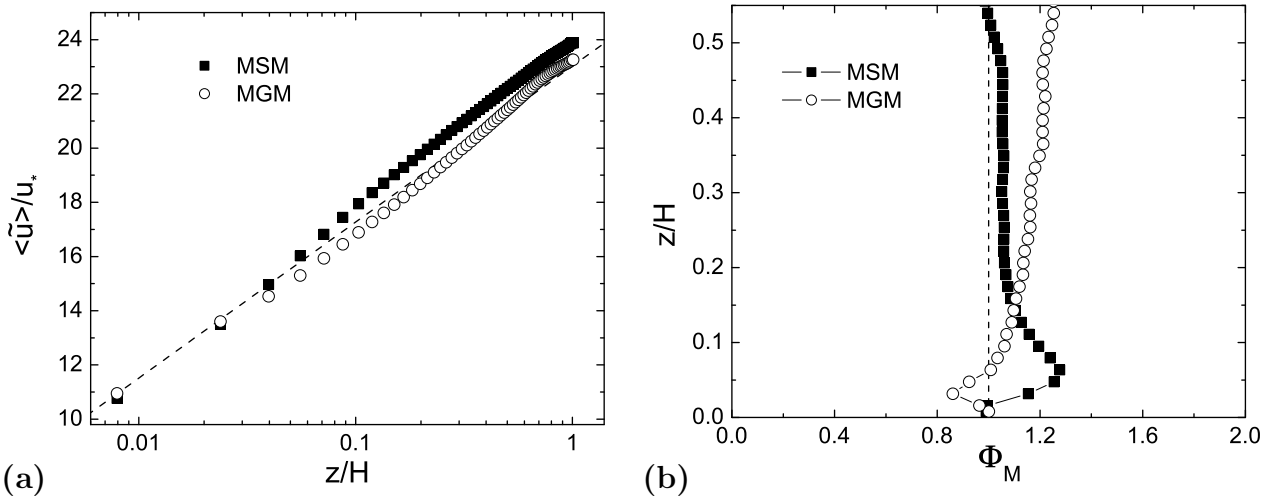

Figure 1: Comparison of results obtained from the 64^3 simulations of the neutral ABL case using the MSM and the MGM: (a) normalized mean resolved streamwise velocity profiles in a semi-logarithmic scale; (b) nondimensional vertical gradient of the mean resolved streamwise velocity versus the normalized height above the surface. The dashed line corresponds to the classical log-law.

The log-law profile, which was first published by von Kármán in 1931, is a semi-empirical relationship used to describe the vertical distribution of horizontal wind speeds above the surface within a turbulent boundary layer. It states that the mean streamwise velocity at a certain point in a turbulent boundary layer is proportional to the logarithm of the distance from that point to the surface. Established later, the Monin-Obukhov similarity theory, which includes thermal effects, has been experimentally confirmed in a number of field experiments starting with the Kansas experiment (Businger et al., 1971), and represents one of the most firmly established results against which new SGS models should be compared. An example of the wind speed profile in neutral cases can be written as the well-known log-law formulation: $< \widetilde{u} >= \frac{u_*}{\kappa} \ln\left(\frac{z}{z_0}\right)$. Aerodynamic roughness, z_0, is necessarily non-zero because the log-law does not apply to the viscous and roughness sublayers. The log-law is a good approximation for the velocity profile of ABL turbulence in the surface layer, which occupies the lowest $\sim 10-15\%$

of the flow in ABL. Figure 1(a) compares the mean streamwise velocity profiles obtained using the MSM and the MGM at the resolution of 64^3. The results obtained using the MSM are consistent with other studies (e.g., Porté-Agel et al., 2000); and it is clear that the MSM leads to mean velocities larger than the ones predicted by the log-law. In the surface layer, the MGM is more effectively able to deliver a logarithmic profile, and the departure of the wind-speed profile from the log-law lessens as the simulation resolution increases (see also Lu and Porté-Agel, 2010).

To more rigorously evaluate model performance, one may examine the values of the nondimensional vertical gradients of the resolved streamwise velocity as a function of vertical position. The nondimensional vertical gradient of the mean resolved streamwise velocity is defined as

$$\Phi_M = \frac{\kappa z}{u_*} \frac{\partial < \widetilde{u} >}{\partial z} \ . \tag{11}$$

On the basis of experimental results and dimensional analysis (e.g., von Kármán, 1931; Businger et al., 1971; Stull, 1988), it has been found in neutral cases that $\Phi_M = 1$ for all z in the surface layer. In this way, the logarithmic-layer mismatch can be manifested more clearly and can help quantitatively evaluate model performance. Figure 1(b) shows the values of the nondimensional vertical gradient of the mean resolved streamwise velocity as a function of vertical position. In line with other studies (e.g., Mason and Thomson, 1992; Porté-Agel et al., 2000), the MSM yields the value of Φ_M in the lowest 10% of the flow is substantially larger (maximum relative error: $\sim 30\%$) than the theoretical value of 1. The MSM is still too dissipative, removes too much kinetic energy from the resolved field, and thus allows for excessive shear in the surface layer, which bears a large value of Φ_M. Note that although the gradient is better predicted by the MSM at higher levels ($z/H > 0.15$), the velocity magnitude is higher as shown in figure 1(a). Recall that the similarity profile is only applicable to the lowest $\sim 10 - 15\%$ of the flow in ABL. Comparatively, in the surface layer, the MGM yields a value of Φ_M that remains close to 1 (maximum relative error: $\sim 15\%$), indicative of the expected logarithmic velocity profile. More details can be found in Lu and Porté-Agel (2010).

For the scalar counterpart, one may examine the values of the nondimensional vertical gradients of the mean resolved scalar concentration as a function of vertical position. That nondimensional scalar gradient is defined as

$$\Phi_\theta = \frac{\kappa z}{\theta_*} \frac{\partial < \widetilde{\theta} >}{\partial z} \ . \tag{12}$$

It has been well documented (e.g., Businger et al., 1971; Stull, 1988) that, in neutral cases, $\Phi_\theta = 0.74$ for all z in the surface layer. The nondimensional vertical gradient of the mean resolved scalar concentration obtained using the MSM with two constant Sc_{sgs} values, shown in figure 2, possesses the same general features as the velocity field counterpart. Consistent

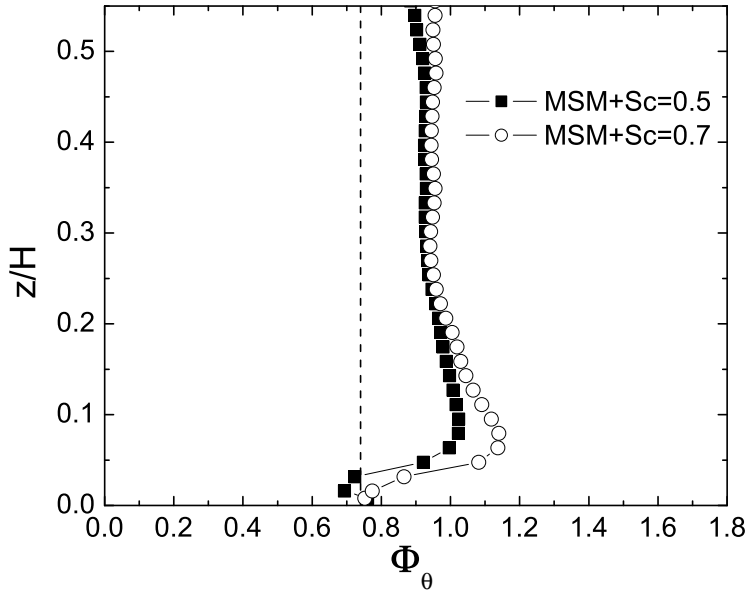

Figure 2: Nondimensional vertical gradient of the mean resolved scalar concentration obtained from the 64^3 simulations of the neutral ABL case using the MSM with two constant Sc_{sgs} values. The dashed line corresponds to the classical log-law.

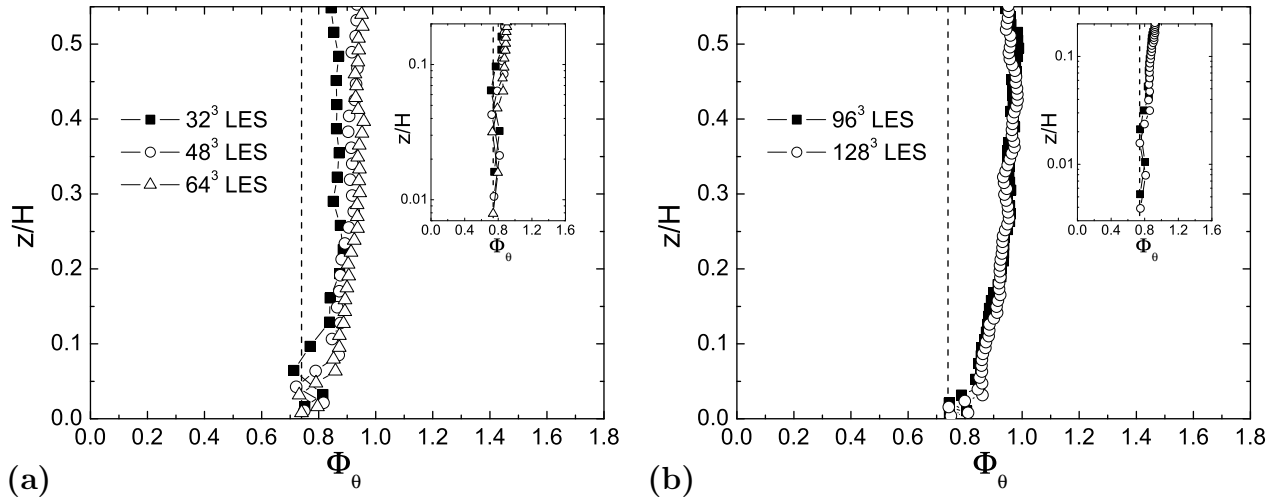

Figure 3: Nondimensional vertical gradient of the mean resolved scalar concentration versus the normalized height above the surface: (a) results from low-resolution simulations of the neutral ABL case; (b) results from high-resolution simulations of the neutral ABL case. The dashed line corresponds to the classical log-law. The right corner plot is a zoomed view of the surface layer and has a log scale in the vertical direction.

with others (e.g., Mason and Thomson, 1992), our current study also reveals that the departure of Φ_θ from the value of 0.74 remains in our simulations. Similar overshoots in Φ_θ have been reported when other eddy-diffusivity approaches were in play (e.g., Sullivan et al., 1994; Porté-

Agel, 2004). Figure 3 presents the nondimensional vertical gradient of the mean resolved scalar concentration profile obtained from different resolution simulations using the new model. Clearly, the MGM yields much better values of Φ_θ, and the results show little sensitivity to grid resolution. We note that the 32^3 simulation delivers values of Φ_θ that are slightly closer to the expected value. This could be due to the effect of increased numerical diffusions at coarse resolutions. Further, the MGM slightly overestimates Φ_θ at the second grid point (with the highest value being about 0.83), and adjusts it back at the third grid point. We note that Porté-Agel (2004) has examined the combination of the dynamic eddy-viscosity model and the dynamic eddy-diffusivity model (e.g., Germano et al., 1991; Moin et al., 1991), and it yields a value of Φ_θ that is quite small (~ 0.6) near the ground, and increases sharply (to ~ 0.9) in the surface layer.

4.2 Power spectra

Power spectrum of scalar fields exhibits the inertial subrange and the dissipation range. In the inertial range, spectrum shows to follow the $-5/3$ power-law scaling (e.g., Sagaut, 2006); particularly in a neutral ABL flow, the inertial subrange should extend for a range of relatively small scales, $k_1 \gtrsim z^{-1}$, where z is the height and k_1 is the streamwise wavenumber. Note that the dissipation range is not resolved in our LESs of high-Reynolds-number turbulent flow; therefore, this range is not considered.

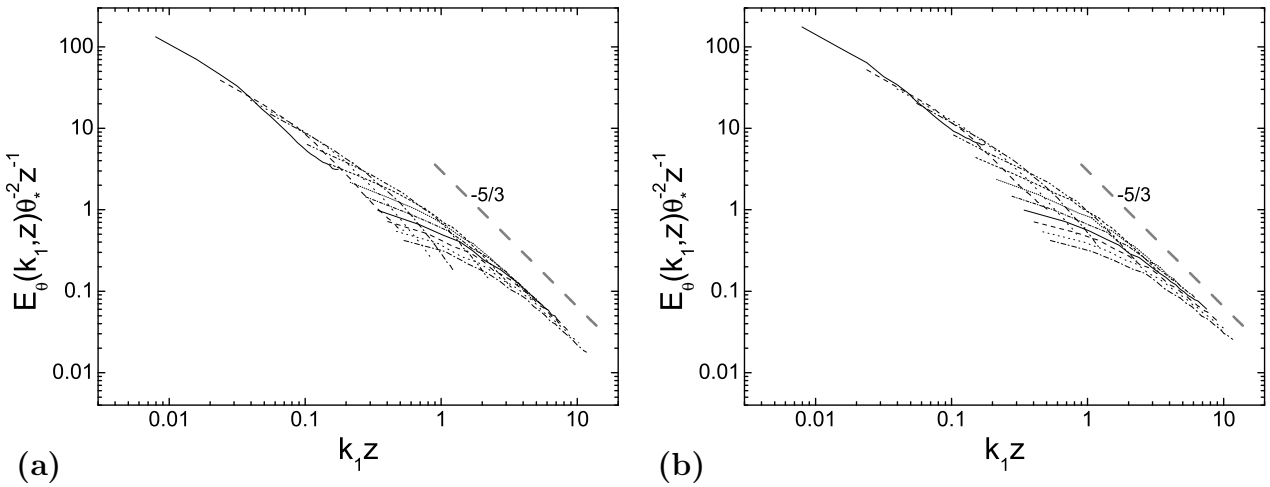

Figure 4: Averaged nondimensional 1-D spectra of the resolved scalar concentration obtained from the 64^3 simulations of the neutral ABL case using the MSM with two constant Sc_{sgs} values: (a) $Sc_{sgs} = 0.5$ and (b) $Sc_{sgs} = 0.7$. Normalized heights (z/H) increase approximately from 0.008 to 0.5. The slope $-5/3$ is also shown.

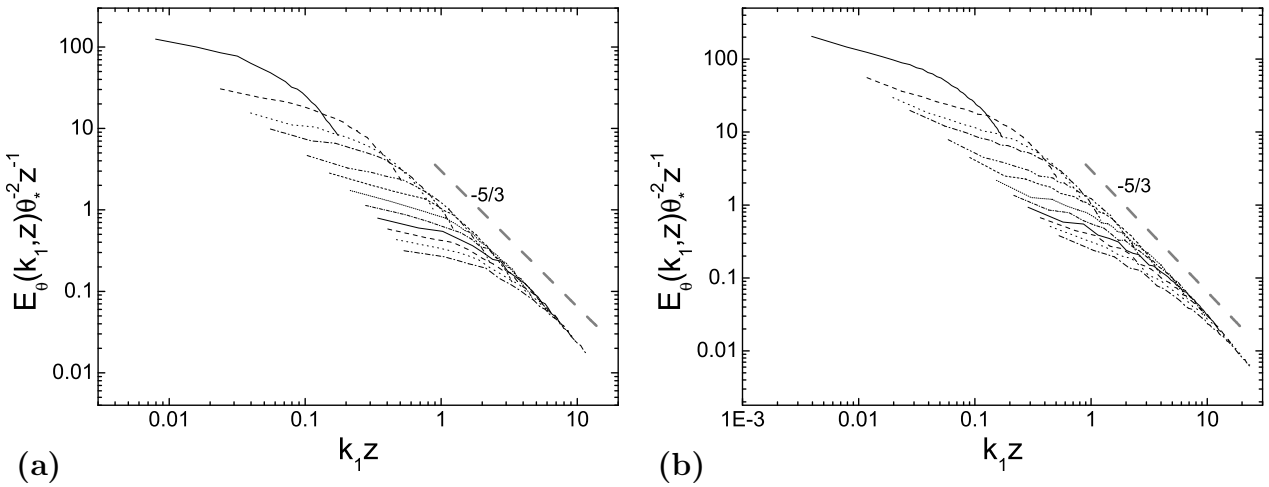

Figure 5: Averaged nondimensional 1-D spectra of the resolved scalar concentration obtained from (a) the 64^3 simulation of the neutral ABL case; and (b) the 128^3 simulation of the neutral ABL case. Normalized heights (z/H) increase approximately from (a) 0.008 to 0.5 or (b) 0.004 to 0.5. The slope $-5/3$ is also shown.

Figure 4 shows the power spectra of the resolved scalar concentration obtained from the 64^3 simulations using the MSM with two constant Sc_{sgs} values. The spectra are calculated from one-dimensional Fourier transforms that are then averaged in the spanwise direction and also in time. In order to check for a possible collapse of the curves in the inertial subrange, they are normalized by $\theta_*^2 z$, and are plotted against $k_1 z$. For relatively small scales ($k_1 z \gtrsim 1$), at which the $-5/3$ power-law scaling arguments are expected to hold, the spectra show a good collapse. In the surface layer, where most of the resolved scales fall outside of the inertial subrange, the spectra drop rapidly, especially for the case with $Sc_{sgs} = 0.5$, indicating that this eddy-diffusivity approach yields excessive dissipation. Moreover, Porté-Agel (2004) has shown that near the surface, the standard dynamic closure (e.g., Germano et al., 1991; Moin et al., 1991) yields spectra whose slopes are too flat and have an unrealistic pile-up of scalar variance at the smallest resolves scales. Andren et al. (1994) have shown that their tested eddy-viscosity/diffusivity models can yield excessive dissipation or noticeable power density accumulation at small scales. Results obtained using eddy-diffusivity models significantly depend on the values of the model coefficients, especially in the surface layer. The current numerical results also support this statement.

Figure 5 shows the nondimensional one-dimensional power spectra obtained from the simulations using the new model at two resolutions (64^3 and 128^3). The MGM is evidently capable of achieving the $-5/3$ power-law scaling in the inertial subrange. In the surface layer, a comparison of these new-model results to the results obtained using the MSM with two Sc_{sgs} values

reveals two major improved features: the MGM yields larger magnitudes in the power containing range (low modes), and is clearly less dissipative at the filter scales. Thus, the MGM could better reproduce the rate of transfer of scalar variance toward the subgrid scales. Also, as expected in LES, the increase of grid resolution will yield an extension of the resolved portion of the inertial subrange.

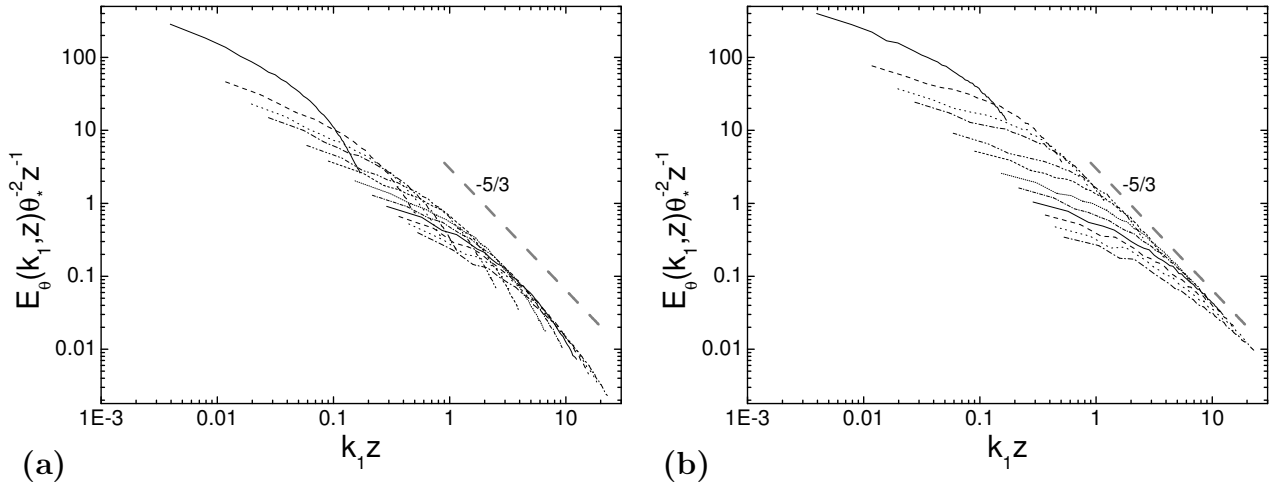

Figure 6: Averaged nondimensional 1-D spectra of the resolved scalar concentration obtained from the 128^3 simulation of the neutral ABL case using different values of $C_{\varepsilon\theta}$: (a) $C_{\varepsilon\theta} = 0.4$ and (b) $C_{\varepsilon\theta} = 2.0$. Normalized heights ($z/H$) increase approximately from 0.004 to 0.5. The slope $-5/3$ is also shown.

In order to investigate the sensitivity of the simulation results to the value of the model coefficient, $C_{\varepsilon\theta}$, additional simulations have been performed. The simulation results reveal that varying $C_{\varepsilon\theta}$ from 0.4 to 2.0 leads to a change in the nondimensional gradient, Φ_θ, from 0.6 to 0.9 (not shown here). Figure 6 presents the nondimensional power spectra obtained using $C_{\varepsilon\theta} = 0.4$ and $C_{\varepsilon\theta} = 2.0$. Excessive dissipation is observed for lower values of the coefficients, and higher values yield less dissipation. Optimal performance can be achieved around $C_{\varepsilon\theta} = 1.0$, which is derived on the basis of theoretical arguments (as shown in section 2) and used in this study.

4.3 Second-order statistics

Figure 7 shows the vertical distributions of the normalized total and partial (resolved and subgrid-scale) shear stresses, and the normalized total and partial wall-normal fluxes obtained from the 128^3 simulation. It also includes the normalized SGS stresses and SGS fluxes obtained from two coarser grids (64^3 and 96^3). As expected, the coarser resolution simulations yield the SGS stresses and the SGS fluxes that are larger in magnitude than the higher resolution counterparts. The simulated flow is driven by a constant pressure gradient, and a constant

surface flux is imposed on the flow; therefore, in the absence of viscous effects, the magnitude of the normalized total turbulent stress and the magnitude of the total turbulent flux decrease linearly from ± 1 at the surface, respectively, to 0 at the top. The similarity between the characteristics of the total turbulent stress and the total turbulent flux has been reported by direct numerical simulation (DNS) studies (e.g., Kim and Moin, 1987), indicating that productions of scalar fluctuations also take place intermittently just as that of velocity fluctuations. Also the near-linear feature of the total turbulent flux is in good agreement with both DNS results (e.g., Kim and Moin, 1987; Kong et al., 2000) in the logarithmic region, and LES results (Porté-Agel, 2004) of a neutral ABL flow. These results also serve as a confirmation of stationarity and momentum conservation of the scheme.

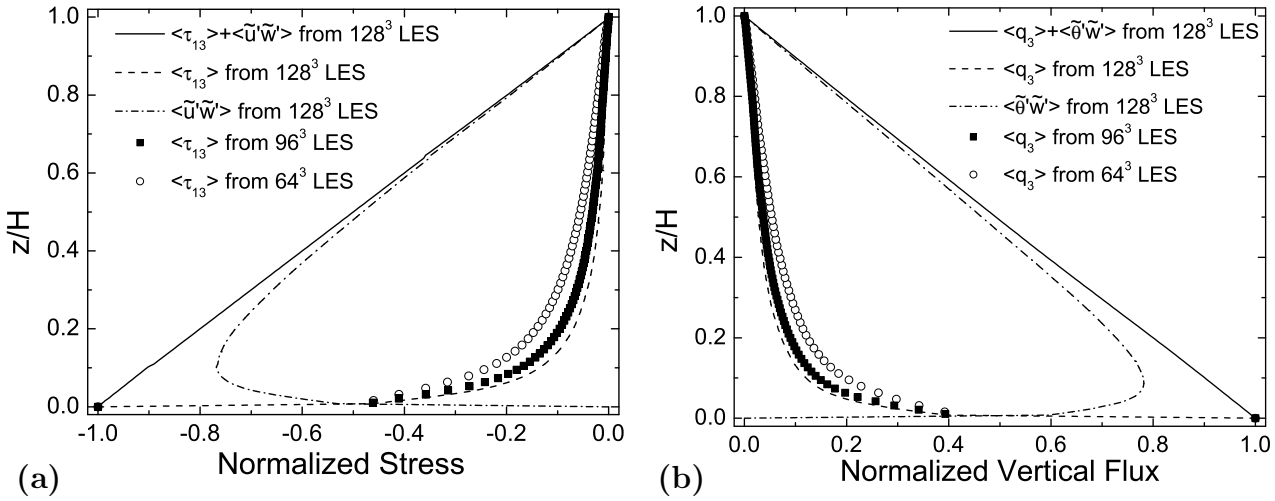

Figure 7: Vertical distributions, in the neutral ABL, of the normalized total and partial (subgrid-scale and resolved): (a) shear stresses and (b) wall-normal fluxes.

Figure 8(a) shows the vertical distributions of the normalized resolved scalar variance obtained from the 128^3 simulation using the MGM, as well as the 64^3 simulations using the MGM and the MSM with two constant Sc_{sgs} values. Lu and Porté-Agel (2010) have shown that differences can be observed between resolved vertical velocity variances obtained from different resolution simulations: an increase in resolution leads to a larger resolved vertical velocity variance. In contrast, horizontal velocity components are mostly dominated by larger (resolved in LES) eddies, and the scalar field bears the same feature as shown in the power spectra (Fig. 5). Consequently, the results stemming from the new model show weak grid-resolution dependence, even if the resolved scalar variance obtained from the 128^3 case is slightly larger. Similar weak grid-resolution dependence has also been revealed previously (Porté-Agel, 2004) from results using standard dynamic eddy-viscosity/diffusivity models and scale-dependent dynamic eddy-viscosity/diffusivity models. Moreover, in line with the power-spectrum results (Fig. 4 and

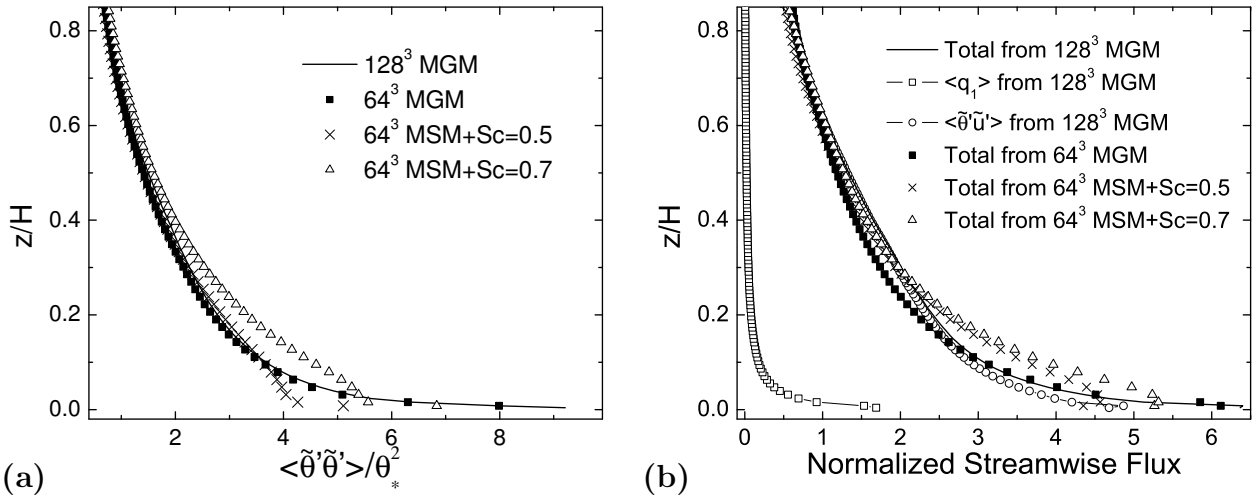

Figure 8: Vertical distributions, in the neutral ABL, of the normalized: (a) variance of the resolved scalar concentration, and (b) total and partial (subgrid-scale and resolved) streamwise fluxes.

Fig. 5), the MGM clearly yields larger scalar variance at the bottom of the boundary layer.

Figure 8(b) shows the normalized total and partial (resolved and subgrid-scale) streamwise fluxes obtained from the 128^3 simulation using the MGM and the normalized total streamwise fluxes obtained from the 64^3 simulations using the MGM and the MSM with two constant Sc_{sgs} values. Unlike the normalized wall-normal fluxes, which should be < 1, the normalized streamwise fluxes are > 1 for most regions. Moreover, the scalar fluctuation exhibits high correlations with the streamwise and vertical velocity fluctuations (the high correlation indicates that low-speed streaks are associated with upward motions, which transport scalar concentration upwards); and the magnitudes of the correlation coefficients between the scalar and the streamwise velocity (in a range of $0.7 \sim 0.85$, not shown here) are slightly higher than those between the scalar and the vertical velocity (in a range of $0.6 \sim 0.7$, not shown here).

5 Stable atmospheric boundary layer

Further, we implement the MGM in a horizontally homogeneous stable boundary layer (SBL) case. The setup is based on an LES inter-comparison study as part of the Global Energy and Water Cycle Experiment Atmospheric Boundary Layer Study (GABLS) initiative. This LES intercomparison case study, described in detail by Beare et al. (2006), represents a typical moderately stable, quasi-equilibrium ABL, similar to those commonly observed over polar regions and equilibrium nighttime conditions over land in mid-latitudes. In summary, the boundary layer is driven by an imposed, uniform geostrophic wind of $U_g = 8\,[\mathrm{m/s}]$; the Coriolis parameter

is set to $f_c = 1.39 \times 10^{-4}$ [rad/s]; the initial potential temperature profile consists of a mixed layer (with potential temperature 265 [K]) up to 100 [m] with an overlying inversion of strength 0.01 [K/m], and the surface (ground level) potential temperature is reduced at a prescribed surface cooling rate of 0.25 [K/h]. The height of the computational domain is $H = 400$ [m]. As suggested by Stoll and Porté-Agel (2008), to provide a larger range of scales (better able to capture larger buoyancy waves), the horizontal domain is twice the horizontal domain used in Beare et al. (2006), thus $L_x = L_y = 800$ [m]. We carried out simulations with resolutions of $N_x \times N_y \times N_z = 64 \times 64 \times 64$, $80 \times 80 \times 80$, $96 \times 96 \times 96$, and $128 \times 128 \times 128$. Different from the constant surface flux imposed in the neutral ABL case, the surface heat flux is computed through the application of the similarity theory: $q_3|_w = \frac{u_* \kappa \left(\theta_s - \widetilde{\theta}\right)}{\ln(z/z_0) - \Psi_H}$, where θ_s is the surface (ground level) potential temperature, and Ψ_H is the stability correction for heat. Following the recommendations of the GABLS study, we adopt the roughness length $z_0 = 0.1$ [m], $\Psi_M = -4.8\frac{z}{L}$ and $\Psi_H = -7.8\frac{z}{L}$, where L is the local Obukhov length. A Rayleigh damping layer above 300 [m] is used following the GABLS case description. More details can be found in Beare and MacVean (2004); Beare et al. (2006); Basu and Porté-Agel (2006); Stoll and Porté-Agel (2008); Lu and Porté-Agel (2011).

5.1 Wind speed and potential temperature

Figure 9 shows the mean profiles of the resolved wind speed and potential temperature. Averaging is performed both horizontally and over the last hour of simulation. Current simulation results are also directly compared with the 80^3 simulation results performed by Basu and Porté-Agel (2006). A low-level jet peaking appears clearly near the top of the boundary layer, as predicted by Nieuwstadt's theoretical model (e.g., Nieuwstadt, 1985) and observed previously in simulations (e.g., Beare et al., 2006; Basu and Porté-Agel, 2006; Stoll and Porté-Agel, 2008). Also in agreement with other GABLS results, the MGM delivers a general decrease of boundary-layer depth, an enhancement of positive curvature in potential temperature in the interior of the SBL, and an increase in jet strength with increased resolution. The current 64^3 simulation has already yielded a boundary-layer depth similar to that of the 80^3 simulation results performed using a local dynamic model (Basu and Porté-Agel, 2006).

The Ekman spiral refers to a structure of currents or winds near a horizontal boundary in which the flow direction rotates as one moves away from the boundary. The laminar solution produces a surface wind parallel to the surface-stress vector and at 45° to the geostrophic wind, a flow angle that is somewhat larger than that observed in real conditions. Figure 10 presents a surface flow angle of approximately 35°, which is in good agreement with most SBL cases (e.g., Kosovic and Curry, 2000; Basu and Porté-Agel, 2006).

In SBL simulations, the nondimensional velocity gradient, Φ_M, and the nondimensional

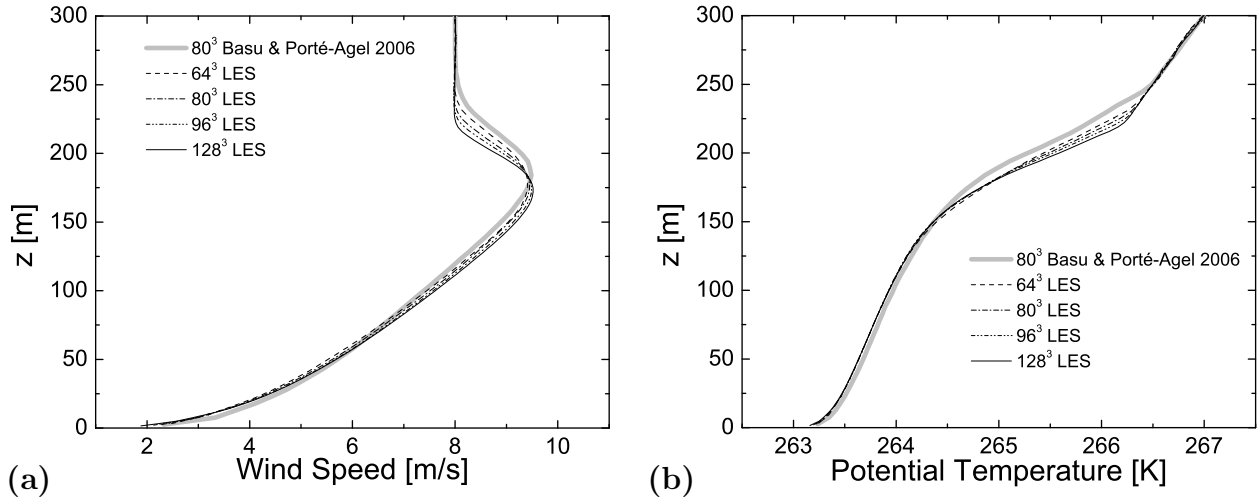

Figure 9: Mean (a) wind speed and (b) potential temperature obtained from different resolution simulations of the GABLS case.

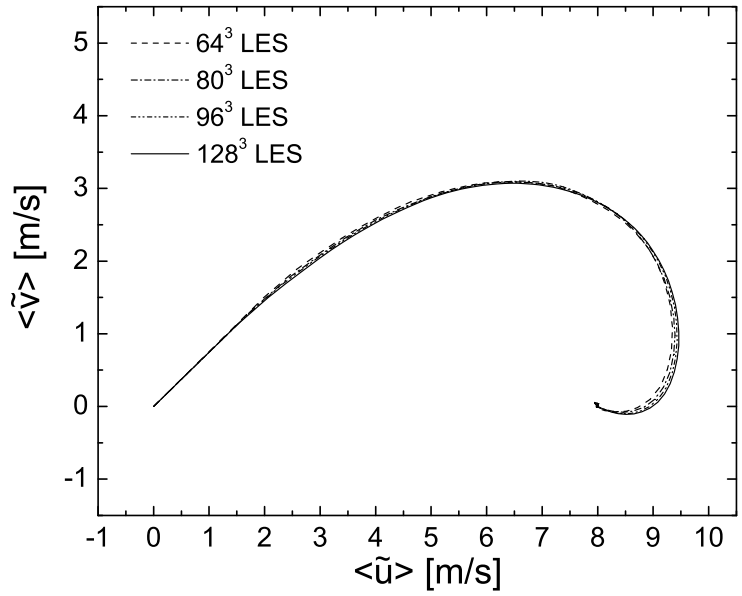

Figure 10: Wind hodographs obtained from different resolution simulations of the GABLS case using the MGM.

temperature gradient, Φ_θ, are key parameters for surface parameterizations in large-scale models and in assessments of SGS models. Owing to the existence of non-zero mean spanwise velocity component, the definition equation (11) is modified as

$$\Phi_M = \frac{\kappa z}{u_*}\sqrt{\left(\frac{\partial < \widetilde{u} >}{\partial z}\right)^2 + \left(\frac{\partial < \widetilde{v} >}{\partial z}\right)^2}\ . \tag{13}$$

In the surface layer, Φ_M and Φ_θ are usually parameterized as functions of z/L. For instance,

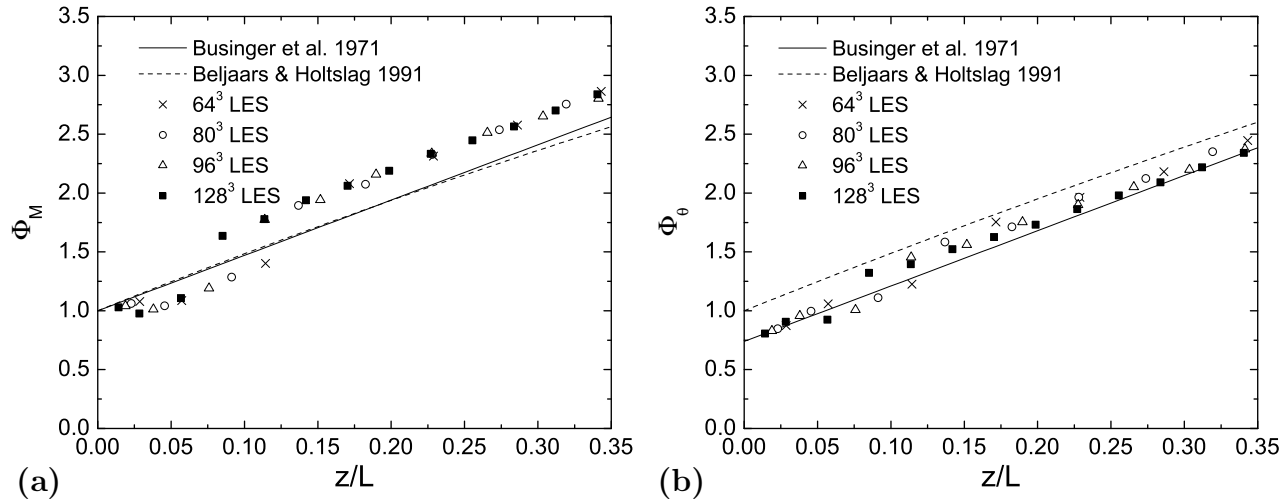

Figure 11: Nondimensional (a) velocity gradient and (b) temperature gradient obtained from different resolution simulations of the GABLS case. The solid and dashed lines correspond to the formulations according to equations (14) and (15).

the well-known linear relations (Businger et al., 1971; Stull, 1988)

$$\Phi_M = 1 + 4.7\frac{z}{L}, \quad \Phi_\theta = 0.74 + 4.7\frac{z}{L}\ , \tag{14}$$

and nonlinear relations derived from Beljarrs and Holtslag (1991)

$$\begin{aligned} \Phi_M &= 1 + \tfrac{z}{L}\left(a + be^{-\frac{dz}{L}}\left(1 + c - \tfrac{dz}{L}\right)\right), \\ \Phi_\theta &= 1 + \tfrac{z}{L}\left(a\sqrt{1 + \tfrac{2}{3}\tfrac{az}{L}} + be^{-\frac{dz}{L}}\left(1 + c - \tfrac{dz}{L}\right)\right), \end{aligned} \tag{15}$$

where the coefficients are $a = 1$, $b = 2/3$, $c = 5$ and $d = 0.35$. These formulations are plotted along with the LES Φ_M and Φ_θ results as functions of z/L in figure 11. The points are from the lowest 40 m of the simulation domain. In general, all the simulation results agree quite well with the empirical relations. Consistent with model performance in the neutral ABL case (Lu and Porté-Agel, 2010), the nondimensional velocity gradient is slightly underestimated for the lowest two to three grid points. It is likely to be associated with the slightly excessive dissipation characteristics of the model. With the coupling of the velocity field and the scalar field, the computed nondimensional scalar gradient matches the similarity profiles remarkably well. In the bulk of the surface layer the results have better agreement with equation (14) than equation (15).

5.2 Turbulent fluxes

Figure 12 shows the mean total and partial (SGS and resolved) profiles of vertical momentum flux and buoyancy flux obtained from the 128^3 simulation. The dotted lines show the resolved

fluxes, and the dashed lines denote the SGS contribution. As would be anticipated, near the ground the SGS contribution is much larger than its resolved counterpart. In the GABLS intercomparison study, there is a spread between the total momentum and buoyancy flux profiles simulated using different models. In particular, the magnitude of the surface momentum flux ranges from 0.06 to 0.08 $[\mathrm{m}^2/\mathrm{s}^2]$, and the magnitude of the surface buoyancy flux ranges from 3.5 to 5.5 $\times 10^{-4}$ $[\mathrm{m}^2/\mathrm{s}^3]$. The current simulation results fall in the ranges.

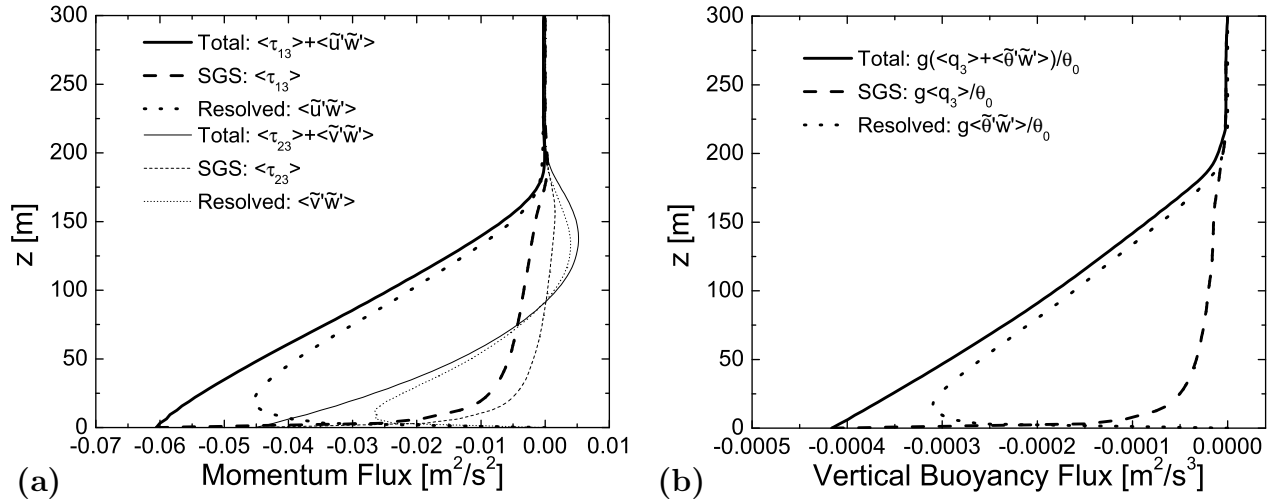

Figure 12: Mean total and partial (subgrid-scale and resolved) (a) momentum flux profiles and (b) buoyancy flux profiles corresponding to the 128^3 simulation of the GABLS case using the MGM.

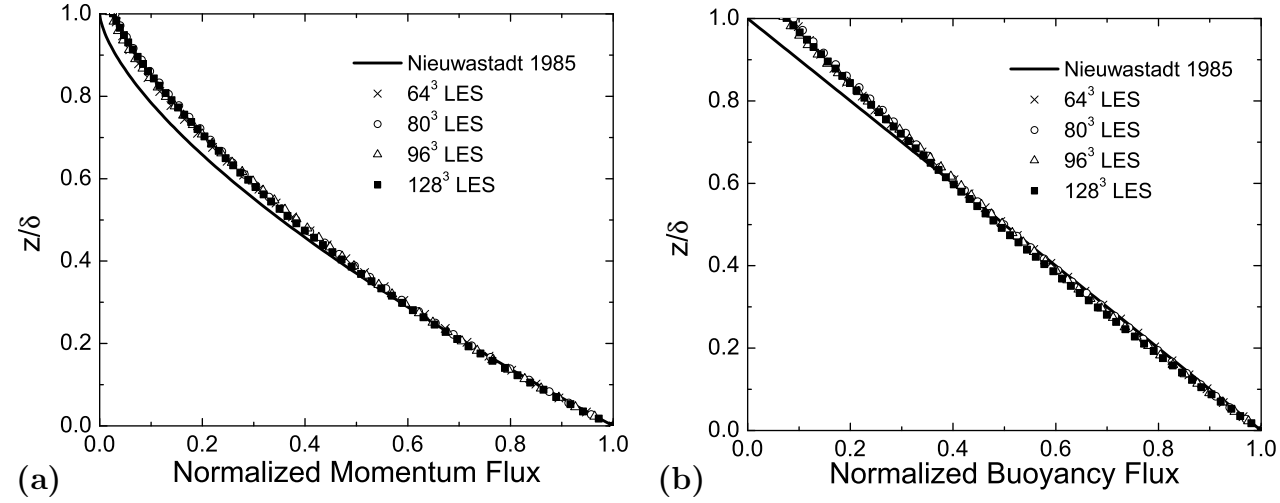

Figure 13: Mean normalized total (a) momentum flux profiles and (b) buoyancy flux profiles obtained from different resolution simulations of the GABLS case.

It is interesting to explore the normalized flux profiles as shown in figure 13. Nieuwstadt's analytical model (Nieuwstadt, 1985) predicts that the total buoyancy flux, if normalized by its

surface value, should be a linear function of z/δ, where the boundary-layer depth δ is defined as (1/0.95) times the height where the horizontally averaged flux falls to five percent of its surface value (Beare et al., 2006); likewise, the total normalized momentum should follow a 3/2 power law with z/δ. The intercomparison study of Beare et al. (2006) and the studies of Basu and Porté-Agel (2006) and Stoll and Porté-Agel (2008) have shown that high-resolution LESs and advanced models could reproduce the profiles to a high degree of accuracy. It is clear that our results follow the theoretical predictions quite closely at all resolutions.

6 Summary

An extension of the modulated gradient SGS stress model (Lu and Porté-Agel, 2010) to the scalar closure problem has been introduced and tested through an assessment in simulations of neutrally stratified and stably stratified ABL turbulence. The new model assumes that the magnitude of the SGS flux vector is computed as the multiplication of an SGS velocity scale and an SGS scalar concentration scale, and the structure (i.e., the relative magnitude of the vector components) of the SGS flux vector is modeled by the normalized gradient vector, which can be derived from Taylor expansion of the SGS flux. Different from standard gradient models, we use the local-equilibrium hypothesis to estimate the SGS velocity scale and the SGS scalar concentration scale, and adopt clipping procedures to avoid backscatter. This, together with the fact that the model uses only local velocity gradients and local scalar gradients, and does not require extra filtering, makes this model computationally efficient.

We examined the proposed model in simulations of a well-established neutral ABL case and a well-known stable ABL case. These are the first successful LESs of the ABL using an unmixed gradient scheme. It is well known that in the surface layer, where SGS motions contribute to a large fraction of the total turbulent fluxes, LES of the ABL is rather sensitive to the SGS model. Traditional eddy-viscosity/diffusivity models yield deviations from the Monin-Obukhov similarity forms in the surface layer. The deviations are readily observed in the wind and temperature profiles, and to a greater extent in their dimensionless vertical derivatives. The new model presents a significant improvement with respect to simple eddy-diffusivity-type models. In summary, the major conclusions from this paper are: (i) gradient models can undergo modifications that help achieve stable and robust simulations; (ii) the local-equilibrium hypothesis together with a clipping procedure provides reasonable estimations of the SGS velocity scale and the SGS scalar concentration scale; and (iii) the applications of the new model to a passive scalar case in a neutral ABL flow and an active scalar case in a stable ABL flow show the model can achieve the expected similarity profiles in the surface layer, realistic spectral scaling, as well as other important statistical characteristics of ABL

turbulence.

Despite the good performance of the new model, it is important to note that the selected constant values of the model coefficients are based on theoretical arguments, which are strictly valid only in the inertial subrange of high-Reynolds-number turbulence. The optimum values of the model coefficients could vary in complex flow conditions, such as turbulent fields near solid walls, rotating flows, mixing layers, or transitional flows. Possible future model modifications (increasing complexity and computational cost) include the development of dynamic and scale-dependent dynamic procedures to optimize the values of the model coefficients using information of the resolved scales. Moreover, we will develop and assess more advanced modifications (e.g., one-equation models), which could offer alternatives to relax some of the model assumptions, such as the local-equilibrium hypothesis. Future work should also include *a-priori* studies using DNS data, field data, etc., and *a-posteriori* testings of the model in other flow conditions (e.g. isotropic turbulent flows, heterogeneous ABL flows).

7 Acknowledgments

This research was supported by the Swiss National Science Foundation (grant 200021_132122), the US National Science Foundation (grant ATM-0854766), and NASA (grant NNG06GE256). Computing resources were provided by the Minnesota Supercomputing Institute and the Swiss National Supercomputing Centre (under project ID s306).

References

[1] H. Lu and F. Porté-Agel. A modulated gradient model for large-eddy simulation: application to a neutral atmospheric boundary layer. *Phys. Fluids*, 22:015109, 2010.

[2] J. Smagorinsky. General circulation experiments with the primitive equations: I. the basic experiment. *Mon. Weather Rev.*, 91(3):99–164, 1963.

[3] J. A. Businger, J. C. Wynagaard, Y. Izumi, and E. F. Bradley. Flux-profile relationships in the atmospheric surface layer. *J. Atmos. Sci.*, 28:181–189, 1971.

[4] R. B. Stull. *An introduction to Boundary-Layer Meteorology*. Kluwer Academic Publishers, 1988.

[5] P. J. Mason. Large-eddy simulation of the convective atmospheric boundary layer. *J. Atmos. Sci.*, 46(11):1492–1516, 1989.

[6] P. J. Mason and D. J. Thomson. Stochastic backscatter in large-eddy simulations of boundary layers. *J. Fluid Mech.*, 242:51–78, 1992.

[7] P. E. Sullivan, J. C. McWilliams, and C.-H. Moeng. A subgrid-scale model for large-eddy simulation of planetary boundary-layer flows. *Boundary-Layer Meteorol.*, 71(3):247–276, 1994.

[8] B. Kosović. Subgrid-scale modelling for the large-eddy simulation of high-Reynolds-number boundary layers. *J. Fluid Mech.*, 336:151–182, 1997.

[9] F. Porté-Agel, C. Meneveau, and M. B. Parlange. A scale-dependent dynamic model for large-eddy simulation: application to a neutral atmospheric boundary layer. *J. Fluid Mech.*, 415:261–284, 2000.

[10] F. Porté-Agel. A scale-dependent dynamic model for scalar transport in large-eddy simulations of the atmospheric boundary layer. *Boundary-Layer Meteorol.*, 112(1):81–105, 2004.

[11] R. A. Clark, J. H. Ferziger, and W. C. Reynolds. Evaluation of subgrid-scale models using an accurately simulated turbulent flow. *J. Fluid Mech.*, 91(1):1–16, 1979.

[12] S. Liu, C. Meneveau, and J. Katz. On the properties of similarity subgrid-scale models as deduced from measurements in a turbulent jet. *J. Fluid Mech.*, 275:83–119, 1994.

[13] C. W. Higgins, M. B. Parlange, and C. Meneveau. Alignment trends of velocity gradients and subgrid-scale fluxes in the turbulent atmospheric boundary layer. *Boundary-Layer Meteorol.*, 109(1):59–83, 2003.

[14] F. Porté-Agel, C. Meneveau, M. B. Parlange, and W. E. Eichinger. A priori field study of the subgrid-scale heat fluxes and dissipation in the atmospheric surface layer. *J. Atmos. Sci.*, 58:2673–2698, 2001.

[15] H. Lu, C. J. Rutland, and L. M. Smith. A priori tests of one-equation LES modeling of rotating turbulence. *J. Turbul.*, 8(37):1–27, 2007.

[16] P. Sagaut. *Large eddy simulation for incompressible flows.* Springer-Verlag, Berlin Heidelberg, 3rd edition, 2006.

[17] J. Bardina, J. H. Ferziger, and W. C. Reynolds. Improved subgrid scale models for large eddy simulation. *AIAA Paper No. 80-1357*, 1980.

[18] F. K. Chow, R. L. Street, M. Xue, and J. H. Ferziger. Explicit filtering and reconstruction turbulence modeling for large-eddy simulation of neutral boundary layer flow. *J. Atmos. Sci.*, 62:2058–2077, 2005.

[19] B. Vreman, B. Geurts, and H. Kuerten. Large-eddy simulation of the temporal mixing layer using the Clark model. *Theor. Comput. Fluid Dyn.*, 8:309–324, 1996.

[20] B. Vreman, B. Geurts, and H. Kuerten. Large-eddy simulation of the turbulent mixing layer. *J. Fluid Mech.*, 339:357–390, 1997.

[21] H. Lu, C. J. Rutland, and L. M. Smith. A posteriori tests of one-equation LES modeling of rotating turbulence. *Int. J. Mod. Phys. C*, 19:1949–1964, 2008.

[22] E. Pomraning and C. J. Rutland. Dynamic one-equation nonviscosity large-eddy simulation model. *AIAA J.*, 40(4):689–701, April 2002.

[23] C. J. Rutland. Large-eddy simulations for internal combustion engines - a review. *Int. J. Engine Res.*, 12:1–31, 2011.

[24] H. Lu. Assessment of the modulated gradient model in decaying isotropic turbulence. *Theor. Appl. Mech. Lett.*, 1:041005, 2011.

[25] S. G. Chumakov and C. J. Rutland. Dynamic structure subgrid-scale models for large eddy simulation. *Int. J. Numer. Meth. Fluids*, 47:911–923, 2005.

[25] M. Germano, U. Piomelli, and W. H. Cabot. A dynamic subgrid-scale eddy viscosity model. *Phys. Fluids A*, 3(7):1760–1765, July 1991.

[26] P. Moin, K. Squires, W. Cabot, and S. Lee. A dynamic subgrid-scale model for compressible turbulence and scalar transport. *Phys. Fluids*, 3(11):2746–2757, 1991.

[28] C. D. Pierce and P. Moin. A dynamic model for subgrid-scale variance and dissipation rate of a conserved scalar. *Phys. Fluids*, 10:3041, 1998.

[29] B. Knaepen, O. Debliquy, and D. Carati. Subgrid-scale energy and pseudo pressure in large-eddy simulation. *Phys. Fluids*, 14:4235, 2002.

[30] V. Borue and S. A. Orszag. Local energy flux and subgrid-scale statistics in three-dimensional turbulence. *J. Fluid Mech.*, 366:1–31, 1998.

[31] C. B. da Silva and O. Métais. On the influence of coherent structures upon interscale interactions in turbulent plane jets. *J. Fluid Mech.*, 473:103–145, 2002.

[32] N. Park, S. Lee, J. Lee, and H. Choi. A dynamic subgrid-scale eddy viscosity model with a global model coefficient. *Phys. Fluids*, 18:125109, 2006.

[33] D. You and P. Moin. A dynamic global-coefficient subgrid-scale eddy-viscosity model for large-eddy simulation in complex geometries. *Phys. Fluids*, 19:065110, 2007.

[34] C. B. da Silva and J. C. F. Pereira. On the local equilibrium of the subgrid scales: The velocity and scalar fields. *Phys. Fluids*, 17:108103, 2005.

[35] S. S. Girimaji and Y. Zhou. Analysis and modeling of subgrid scalar mixing using numerical data. *Phys. Fluids*, 8:1224, 1996.

[36] J. P. H. Sanders and I. Gökalp. Scalar dissipation rate modelling in variable density turbulent axisymmetric jets and diffusion flames. *Phys. Fluids*, 10:938, 1998.

[37] G. Balarac, H. Pitsch, and V. Raman. Modeling of the subfilter scalar dissipation rate using the concept of optimal estimators. *Phys. Fluids*, 20:091701, 2008a.

[38] C. B. da Silva, S. Rego, and J. C. F. Pereira. Analysis of the viscous/molecular subgrid-scale dissipation terms in les based on transport equations: A priori tests. *J. Turbul.*, 9(25): 1–36, 2008.

[39] A. Yoshizawa and K. Horiuti. A statistically-derived subgrid-scale kinetic energy model for the large-eddy simulation of turbulent flows. *J. Phys. Soc. Jpn.*, 54(8):2834–2839, August 1985.

[40] A. Yoshizawa. Statistical theory for compressible turbulent shear flows, with the application to subgrid modeling. *Phys. Fluids*, 29:2152, 1986.

[41] G. Balarac, H. Pitsch, and V. Raman. Development of a dynamic model for the subfilter scalar variance using the concept of optimal estimators. *Phys. Fluids*, 20:035114, 2008b.

[42] D. K. Lilly. A proposed modification of the Germano subgrid-scale closure method. *Phys. Fluids*, 4(3):633–635, March 1992.

[43] C. Jiménez, F. Ducros, B. Cuenot, and B. Bédat. Subgrid scale variance and dissipation of a scalar field in large eddy simulations. *Phys. Fluids*, 13(6):1748–1754, 2001.

[44] W.-W. Kim and S. Menon. A new dynamic one-equation subgrid-scale model for large eddy simulations. *AIAA Paper 1995-356*, 1995.

[45] A. Andren, A. R. Brown, J. Graf, P. J. Mason, C.-H. Moeng, F. T. M. Nieuwstadt, and U. Schumann. Large-eddy simulation of a neutrally stratified boundary layer: A comparison of four computer codes. *Q. J. R. Meteorol. Soc.*, 120(520):1457–1484, 1994.

[46] J. D. Albertson and M. B. Parlange. Natural integration of scalar fluxes from complex terrain. *Advan. Water Resour.*, 23:239–252, 1999.

[47] R. Stoll and F. Porté-Agel. Effect of roughness on surface boundary conditions for large-eddy simulation. *Boundary-Layer Meteorol.*, 118(1):169–187, 2006a.

[48] R. Stoll and F. Porté-Agel. Dynamic subgrid-scale models for momentum and scalar fluxes in large-eddy simulations of neutrally stratified atmospheric boundary layers over heterogeneous terrain. *Water. Resour. Res.*, 42:W01409, 2006b.

[49] R. Stoll and F. Porté-Agel. Large-eddy simulation of the stable atmospheric boundary layer using dynamic models with different averaging schemes. *Boundary-Layer Meteorol.*, 126(1): 1–28, 2008.

[50] C. Canuto, M. Y. Hussaini, A. Quarteroni, and T. A. Zang. *Spectral methods in fluid dynamics*. Sprnger-Verlag, Berlin Heidelberg, 1988.

[51] H. Kong, H. Choi, and J. S. Lee. Direct numerical simulation of turbulent thermal boundary layers. *Phys. Fluids*, 12(10):2555–2568, 2000.

[52] D. K. Lilly. The representation of small-scale turbulence in numerical simulation experiments. *Proc. IBM Sci. Com. Symp. Environmental Sciences (Yorktown Heights, N.Y.)*, page 167, 1967.

[53] M. Antonopoulos-Domis. Large-eddy simulation of a passive scalar in isotropic turbulence. *J. Fluid Mech.*, 104:55–79, 1981.

[54] J. Kleissl, C. Meneveau, and M. B. Parlange. On the magnitude and variability of subgrid-scale eddy-diffusion coefficients in the atmospheric surface layer. *J. Atmos. Sci.*, 60:2372–2388, 2003.

[55] E. Bou-Zeid, N. Vercauteren, M. B. Parlange, and C. Meneveau. Scale dependence of subgrid-scale model coefficients: an a priori study. *Phys. Fluids*, 20, 2008.

[56] T. von Kármán. Mechanical similitude and turbulence. *Tech. Mem., No. 611, Washington D.C., NACA*, 1931.

[57] J. Kim and P. Moin. Transport of passive scalars in a turbulent channel flow. *Proceedings of the 6th International Symposium on Turbulent Shear Flows, Toulouse, France, 7-9 September 1987 (Spinger-Verlag, Berlin)*, 1987.

[58] R. J. Beare, M. K. MacVean, A. A. M. Holtslag, J. Cuxart, I. Esau, J.-C. Golaz, M. A. Jimenez, M. Khairoutdinov, B. Kosovic, D. Lewellen, T. S. Lund, J. K. Lundquist, A. McCabe, A. F. Moene, Y. Noh, S. Raasch, and P. Sullivan. An intercomparison of large-eddy simulations of the stable boundary layer. *Boundary-Layer Meteorol.*, 118(2):247–272, 2006.

[59] R. J. Beare and M. K. MacVean. Resolution sensitivity and scaling of large-eddy simulations of the stable boundary layer. *Boundary-Layer Meteorol.*, 112(2):257–281, 2004.

[60] S. Basu and F. Porté-Agel. Large-eddy simulation of stably stratified atmospheric boundary layer turbulence: A scale-dependent dynamic modeling approach. *J. Atmos. Sci.*, 63:2074–2091, 2006.

[61] H. Lu and F. Porté-Agel. Large-eddy simulation of a very large wind farm in a stable atmospheric boundary layer. *Phys. Fluids*, 23:065101, 2011.

[62] F. T. M. Nieuwstadt. *Turbulence and diffusion in stable environments*, chapter "A model for the stationary, stable boundary layer", pages 149–179. edited by J. C. R. Hunt, Oxford University Press, 1985.

[63] B. Kosovic and J. A. Curry. A large eddy simulation study of a quasi-steady, stably strati ed atmospheric boundary layer. *J. Atmos. Sci.*, 57:1052–1068, April 2000.

[64] A. C. M. Beljarrs and A. A. M. Holtslag. Flux parameterization over land surfaces for atmospheric models. *J. Appl. Meteorol.*, 30:327–341, 1991.